Journal of Biomolecular NMR, 5 (1995) 1–13
ESCOM

J-Bio NMR 219

Three-dimensional structure of ectatomin from *Ectatomma tuberculatum* ant venom

Dmitry E. Nolde, Alexander G. Sobol, Kirill A. Pluzhnikov, Eugene V. Grishin and Alexander S. Arseniev*

Shemyakin and Ovchinnikov Institute of Bioorganic Chemistry, Russian Academy of Sciences, Ul. Mikhukho-Maklaya 16/10, Moscow 117871, Russia

Received 4 May 1994
Accepted 28 July 1994

Keywords: Ectatomin; Pore-forming protein; 2D NMR; Protein structure

Summary

Two-dimensional ^{1}H NMR techniques were used to determine the spatial structure of ectatomin, a toxin from the venom of the ant *Ectatomma tuberculatum*. Nearly complete proton resonance assignments for two chains of ectatomin (37 and 34 amino acid residues, respectively) were obtained using 2D TOCSY, DQF-COSY and NOESY experiments. The cross-peak volumes in NOESY spectra were used to define the local structure of the protein and generate accurate proton–proton distance constraints employing the MARDIGRAS program. Disulfide bonds were located by analyzing the global fold of ectatomin, calculated with the distance geometry program DIANA. These data, combined with data on the rate of exchange of amide protons with deuterium, were used to obtain a final set of 20 structures by DIANA. These structures were refined by unrestrained energy minimization using the CHARMm program. The resulting rms deviations over 20 structures (excluding the mobile N- and C-termini of each chain) are 0.75 Å for backbone heavy atoms, and 1.25 Å for all heavy atoms. The conformations of the two chains are similar. Each chain consists of two α-helices and a hinge region of four residues; this forms a hairpin structure which is stabilized by disulfide bridges. The hinge regions of the two chains are connected together by a third disulfide bridge. Thus, ectatomin forms a four-α-helical bundle structure.

Introduction

Ants are dominant predators in the animal world and many species subdue their prey by injecting venom. Surprisingly, not much is known about the biochemistry of ant venoms. Amongst the 11 subfamilies of ants, only the venom from a limited number of species in five subfamilies has been characterized pharmacologically and chemically (for a review, see Blum (1992)). Many different types of enzymatic (e.g. hyaluronidase, lipase, esterase), hemolytic and toxic activities were found in ant venoms (Schmidt et al., 1986). The venom from the ant *Ectatomma tuberculatum* is the most toxic known to date (Schmidt et al., 1986). In a preceding article (Arseniev et al., 1994) we described the isolation and characterization of ectatomin (Ea), the principal toxic component of *E. tuberculatum* venom.

Ea is a water-soluble protein composed of two chains, A (37 amino acid residues) and B (34 residues), connected by disulfide bonds (a total of 6 cysteine residues are present in the sequences of the A + B chains, but no free sulfhydryl groups were detected). When Ea was first isolated (Arseniev et al., 1994), NMR spectroscopy was used to reveal its polypeptide nature, purity, and the absence of nonpeptide components. Clearly, a prerequisite for further structure–function relationship studies of this biologically active molecule is a knowledge of its detailed spatial structure.

Here we present the structure of Ea in water. Prior to our study, nothing was known about the mechanism of the lethal activity of Ea. An examination of Ea structure and possible rearrangements of the structure led us to suggest that Ea may be a membrane pore former. This hypothesis was tested in experiments on artificial bilayer

*To whom correspondence should be addressed.

membranes and oocytes (Arseniev et al., 1994; Pluzhnikov et al., 1994). In both experiments, the two Ea molecules formed a nonselective cation channel. This finding, and the known spatial structure of Ea in aqueous solution, were employed to propose a model for the insertion of Ea into membranes.

Materials and Methods

Ectatomin was isolated and purified as described previously (Arseniev et al., 1994). For the NMR experiments, 3 mg of lyophilized protein was dissolved in 150 µl of water (including 10% D_2O as internal lock) to yield a final concentration of 2.5 mM at pH 3.0. The sample was later lyophilized, dissolved in 150 µl of D_2O and used for measuring exchange rates of amide protons with deuterium.

To facilitate water signal suppression, all NMR experiments were performed in 5-mm heavy-wall NMR tubes. Two-dimensional ^1H NMR NOESY (relaxation delay 1.2 s, mixing time τ_m = 100 and 200 ms), TOCSY (τ_m = 50 ms) and DQF-COSY spectra were recorded in phase-sensitive mode at 600 MHz (Varian Unity 600 spectrometer) at 10 and 30 °C. The water signal was saturated by continuous irradiation during the relaxation delays of all 2D experiments and the mixing period of the NOESY spectra. Acquisition times were 0.256 s for the TOCSY and NOESY and 0.512 s for the DQF-COSY, while the spectral width was 8000 Hz for all experiments. The number of complex points in the t_1 dimension was 512 for the DQF-COSY, 300 for the TOCSY and 256 for the NOESY. The data were zero-filled, then Fourier transformed to 2048 real points in both dimensions. Chemical shifts were measured relative to the water resonance, which was arbitrarily taken as 4.95 ppm at 10 °C and 4.75 ppm at 30 °C.

Sequence-specific resonance assignments were made using the standard methods (Wüthrich, 1986). Nonsequential NOESY cross peaks were assigned by the program EASY (Eccles et al., 1991). Unambiguously assigned NOESY cross peaks were used for structure calculations (see below). At different stages of these calculations, NOESY cross peaks were checked against the structure and the list of unambiguously assigned cross peaks was updated and corrected if necessary (see the Results section).

For a qualitative estimation of the exchange rates between the NH protons and the solvent deuterons, a NOESY spectrum (τ_m = 200 ms) was recorded in 18 h at 30 °C immediately after Ea was dissolved in D_2O. NH protons which gave detectable signals in this spectrum were considered to be forming hydrogen bonds.

The line widths of the NH resonances prevented evaluation of spin–spin coupling constants of vicinal HN-$C^\alpha H$ protons in the phase-sensitive DQF-COSY spectrum. The rotamers around the $C^\alpha H$-$C^\beta H$ bond were assessed by qualitative evaluation of $C^\alpha H$-$C^\beta H$ vicinal coupling constants. If a pair of $C^\alpha H$ and $C^\beta H$ protons gave a strong nonoverlapped cross peak in the DQF-COSY spectrum, we considered the $C^\beta H$ proton to be trans oriented relative to $C^\alpha H$ (vicinal $C^\alpha H$-$C^\beta H$ coupling constant greater than 10 Hz). This corresponds to $\chi^1 = -60$ or 180°.

Cross-peak integral intensities were measured in NOESY spectra at 10 °C recorded in H_2O (10% D_2O) by a lineshape (Denk) integration routine using the EASY program. Only cross peaks which had an integration error < 20% were used for structure calculation. We corrected for the presence of 10% D_2O; integral intensities of cross peaks between NH and other protons were divided by 0.9, and cross peaks between pairs of NH protons by 0.81.

The spatial structure calculations of Ea proceeded in several rounds:

(1) analysis of local structure with CONFORNMR (Lomize et al., 1990a,b, 1992) to obtain φ, ψ and χ^1 angle constraints;

(2) preliminary structure calculation with the distance geometry program DIANA (Güntert et al., 1991; Güntert and Wüthrich, 1991) using constraints obtained in round (1) and constraints derived from NOESY cross-peak volumes based on '$1/r^6$ calibration' (Barsukov et al., 1992);

(3) computer-aided NOESY cross-peak assignment using conformations from previous rounds;

(4) accurate calculation of upper and lower limits for proton–proton distances from NOESY cross-peak intensities with the program MARDIGRAS (Borgias and James, 1990);

(5) distance geometry calculations with DIANA and stereospecific assignment with GLOMSA (Güntert et al., 1991); then the procedure is repeated from stage 3 until the assignment list is converged;

(6) unrestrained energy minimization with the CHARMm program (Brooks et al., 1988).

The DIANA program (version 1.14), incorporating the REDAC algorithm (Güntert and Wüthrich, 1991), was used for distance geometry calculation. To join the two polypeptide chains, a pseudoresidue was added in the DIANA library file; this pseudoresidue was geometrically equivalent to glycine but with N-C^α, C^α-C and C-N bond lengths 10 times greater than for glycine. The pseudoresidue comprises pseudoatoms which are not involved in van der Waals interactions. For the DIANA calculations, we connected the N-terminal residue of the second chain and the C-terminal residue of the first chain by three pseudoglycine residues. All torsion angles (including ω) of these pseudoresidues were unconstrained.

Four types of constraints were used by DIANA: torsion angle constraints determined from local structure analysis using the CONFORNMR program, disulfide bond con-

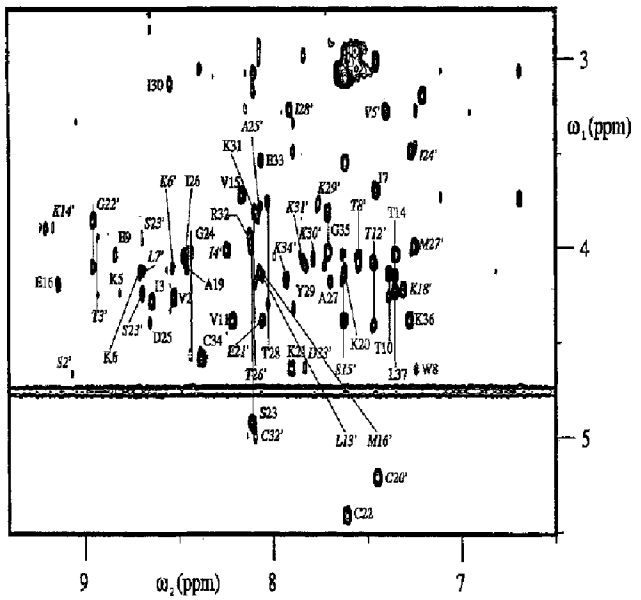

Fig. 1. Fingerprint region of a TOCSY spectrum of Ea in H_2O at 30 °C, pH 3.0, mixing time 50 ms. Assignment of all NH-$C^{\alpha}H$ cross peaks as well as NH-$C^{\beta}H$ cross peaks of serine and threonine residues is shown (a prime after a residue number denotes that the residue belongs to chain B). The unlabeled cross peaks correspond to side-chain resonances of lysine and arginine residues and NH-$C^{\beta}H$ cross peaks of other residues.

straints, hydrogen bond constraints and interproton distance constraints. The locations of disulfide bonds and acceptors for hydrogen bonds involving amide protons were determined after preliminary structure calculation.

Upper and lower interproton distance constraints were calculated from NOESY cross-peak volumes using a '$1/r^6$ calibration' for the first DIANA round, and employing MARDIGRAS in the following rounds.

Some distance constraints obtained with MARDIGRAS depend on the initial model. Accordingly, 10 sets of distance constraints were calculated with MARDIGRAS from the 10 best initial DIANA structures. A single consensus set of distance constraints was compiled, comprising constraints that were present in at least seven of the above sets; this consensus set was used in all subsequent calculations.

Finally, the 20 best DIANA structures were refined with CHARMm (version 21.1.7b). An adopted basis Newton–Raphson minimization (1000 steps) was performed without any constraints. The topology and parameter files used (AMINOH.BIN and PARM21A.BIN) included all hydrogens; a dielectric constant of 80 and a distance-dependent dielectric approximation (RDIE option) were used.

The theoretical NOESY spectrum was calculated using the program CORMA (Keepers and James, 1984). The measures of the agreement between theoretical and experimental NOESY cross-peak intensities are R and R^x factors, defined as

$$R = \sum_k \left| a_o^k - a_c^k \right| \; / \; \sum_k a_o^k$$

$$R^x = \sum_k \left| (a_o^k)^{1/6} - (a_c^k)^{1/6} \right| \; / \; \sum_k (a_o^k)^{1/6}$$

where the subscripts denote calculated (c) and observed (o) cross-peak intensities.

Circular dichroism experiments were carried out with a J-500 spectrometer (Jasco) with 0.1 mm path length quartz cells. The protein concentration was 1 mg/ml, both in water and in methanol.

Results

^1H NMR assignments

The cross-peak assignments were made according to standard techniques, by identifying the amino acid spin systems in the DQF-COSY and TOCSY (Fig. 1) spectra at 30 °C, followed by sequential resonance assignments using the $d_{\alpha N}$, $d_{\beta N}$ and d_{NN} connectivities in the NOESY spectra (τ_m = 200 ms) at 10 °C (Fig. 2) and 30 °C. The resulting assignments are listed in Table 1. Sequential NOE connectivities and the locations of the slowly exchanging amide protons are summarized in Fig. 3 (a prime after a residue number indicates that the residue belongs to chain B). The assignment was mostly straightforward, except for a few minor problems. The main problem was assigning the signals of five C-terminal residues of chain B. We found two distinct sets of resonances for residues $Lys^{31'}$ and $Cys^{32'}$ (Table 1), indicating the pres-

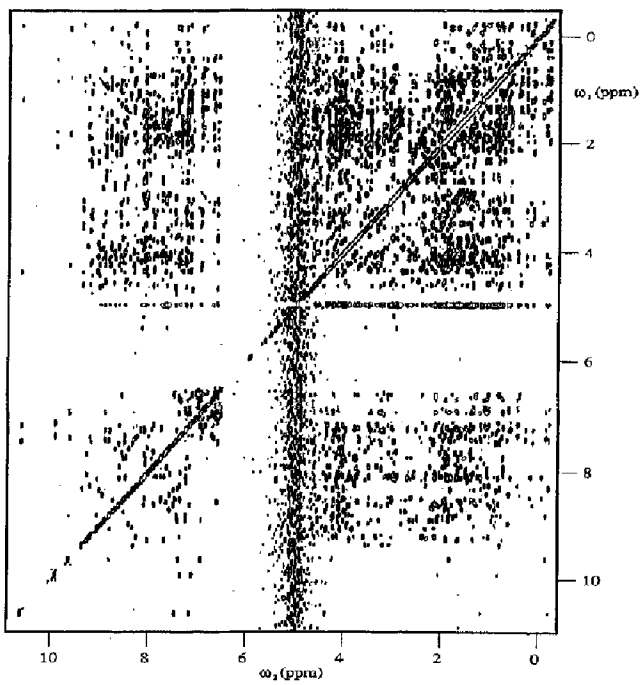

Fig. 2. NOESY spectrum of Ea in H_2O at 10 °C, pH 3.0, mixing time 200 ms.

TABLE 1
^{1}H CHEMICAL SHIFTS OF Ea IN H_2O AT pH 3.0, 10 °C

	Chemical shift (ppm)			
Residue	NH	$C^{\alpha}H$	$C^{\beta}H$	Other protons
Chain A				
Gly[1]	–	3.90		
Val[2]	8.63	4.22	2.06	$C^{\gamma}H$ 0.95, 0.99
Ile[3]	8.81	4.24	1.83	$C^{\gamma 1}H$ *1.68, 0.86*; $C^{\gamma 2}H$ –0.15; $C^{\delta}H$ 0.77
Pro[4]	–	4.53	2.49	$C^{\gamma}H$ *2.07, 1.96*; $C^{\delta}H$ *4.07, 3.38*
Lys[5]	8.90	4.22	*2.08, 1.85*	$C^{\gamma}H$ *1.74, 1.58*
Lys[6]	8.82	4.11	1.84	$C^{\gamma}H$ 1.42; $C^{\delta}H$ 1.70; $C^{\varepsilon}H$ 2.96
Ile[7]	7.43	3.68	1.83	$C^{\gamma 1}H$ 1.29, 1.38; $C^{\gamma 2}H$ 0.26; $C^{\delta}H$ 0.65
Trp[8]	7.25	4.63	*3.27, 3.44*	$N^{\varepsilon 1}H$ 9.64; $C^{\delta 1}H$ 6.93; $C^{\varepsilon 3}H$ 7.48; $C^{\zeta 3}H$ 6.60; $C^{\eta 1}H$ 6.68; $C^{\zeta 2}H$ 7.39
Glu[9]	8.91	4.01	*2.33, 2.17*	$C^{\gamma}H$ 2.58, 2.65
Thr[10]	7.40	4.09	4.23	$C^{\gamma}H$ 1.18
Val[11]	8.31	4.36	1.98	$C^{\gamma}H$ *–0.21, 0.79*
Cys[12]	9.36	4.58	*3.19, 3.06*	
Pro[13]	–	4.31	1.84, 2.44	$C^{\gamma}H$ *2.01, 2.20*; $C^{\delta}H$ *3.54, 3.47*
Thr[14]	7.37	4.00	4.13	$C^{\gamma}H$ 0.43
Val[15]	8.25	3.78	2.32	$C^{\gamma}H$ *1.11, 1.03*
Glu[16]	9.21	4.20	*2.28, 2.38*	$C^{\gamma}H$ 2.13
Pro[17]	–	4.20	*1.77, 2.39*	$C^{\gamma}H$ 1.91, 2.06; $C^{\delta}H$ *3.59, 3.32*
Trp[18]	6.60	4.68	*3.71, 3.01*	$N^{\varepsilon 1}H$ 9.92; $C^{\delta 1}H$ 7.12; $C^{\varepsilon 3}H$ 7.22; $C^{\zeta 3}H$ 6.95; $C^{\eta 1}H$ 6.71; $C^{\zeta 2}H$ 7.35
Ala[19]	8.56	4.11	1.60	
Lys[20]	7.65	4.09	1.72	$C^{\gamma}H$ 1.41; $C^{\delta}H$ 2.03; $C^{\varepsilon}H$ 3.00
Lys[21]	7.92	4.60	*1.98, 2.23*	$C^{\gamma}H$ 1.49, 1.57; $C^{\delta}H$ 1.74; $C^{\varepsilon}H$ 3.23
Cys[22]	7.64	5.39	*3.56, 2.94*	
Ser[23]	8.14	4.96	3.91, 3.95	
Gly[24]	8.51	*4.00, 4.55*		
Asp[25]	8.73	4.36	*2.73, 2.81*	
Ile[26]	8.52	4.04	1.95	$C^{\gamma 1}H$ 1.34, 1.66; $C^{\gamma 2}H$ 1.18; $C^{\delta}H$ 0.91
Ala[27]	7.75	4.18	1.41	
Thr[28]	8.08	3.73	4.28	$C^{\gamma}H$ 1.26
Tyr[29]	7.91	4.33	*3.32, 3.49*	$C^{\delta}H$ 6.94; $C^{\varepsilon}H$ 7.16
Ile[30]	8.60	3.09	1.92	$C^{\gamma 1}H$ 1.29, 2.11; $C^{\gamma 2}H$ 0.83; $C^{\delta}H$ 1.04
Lys[31]	8.11	3.84	1.87	$C^{\gamma}H$ 1.38; $C^{\delta}H$ 1.58, 1.67; $C^{\varepsilon}H$ 2.71, 2.92; $N^{\zeta}H$ 7.66
Arg[32]	8.13	3.90	1.88	$C^{\gamma}H$ *1.41, 1.67*; $C^{\delta}H$ 3.18; $N^{\varepsilon}H$ 7.26
Glu[33]	8.10	3.48	*0.17, –0.07*	$C^{\gamma}H$ *1.21, 1.50*
Cys[34]	8.48	4.50	*2.63, 3.03*	
Gly[35]	7.75	*4.01, 3.76*		
Lys[36]	7.22	4.35	*1.70, 1.49*	$C^{\gamma}H$ 1.89; $C^{\delta}H$ 1.60; $C^{\varepsilon}H$ 2.85
Leu[37]	7.31	4.19	*1.61, 1.79*	$C^{\gamma}H$ 1.78; $C^{\delta}H$ 0.87, 0.96
Chain B				
Trp[1']	–	4.75	*3.36, 3.22*	$N^{\varepsilon 1}H$ 10.62; $C^{\delta 1}H$ 7.45; $C^{\varepsilon 3}H$ 7.26; $C^{\zeta 3}H$ 6.90; $C^{\eta 1}H$ 6.85; $C^{\zeta 2}H$ 7.16
Ser[2']	9.18	4.63	*4.14, 4.43*	
Thr[3']	9.02	3.93	4.22	$C^{\gamma}H$ 1.33
Ile[4']	8.33	3.99	1.81	$C^{\gamma 1}H$ 1.32, 1.41; $C^{\gamma 2}H$ 0.87; $C^{\delta}H$ 0.89
Val[5']	7.49	3.24	2.17	$C^{\gamma}H$ *0.12, 0.89*
Lys[6']	8.61	4.11	2.17, 2.17	
Leu[7']	8.70	4.11	*1.85, 1.57*	$C^{\gamma}H$ 1.94; $C^{\delta}H$ 0.90
Thr[8']	7.59	4.02	4.09	$C^{\gamma}H$ 1.17
Ile[9']	8.41	4.57	1.06	$C^{\gamma 1}H$ 0.88, 1.36; $C^{\gamma 2}H$ 0.62; $C^{\delta}H$ 0.39
Cys[10']	8.96	4.62	*3.92, 2.81*	
Pro[11']	–	4.64	1.99	$C^{\gamma}H$ *2.23, 2.40*; $C^{\delta}H$ 3.50, 3.69
Thr[12']	7.57	4.04	4.42	$C^{\gamma}H$ 1.39
Leu[13']	8.04	4.12	*1.68, 2.31*	$C^{\gamma}H$ 2.13; $C^{\delta}H$ 1.07, 1.36
Lys[14']	9.27	3.88	1.89	$C^{\gamma}H$ 1.35; $C^{\delta}H$ 1.66; $C^{\varepsilon}H$ 2.85
Ser[15']	7.68	4.35	4.01, 4.13	
Met[16']	8.10	4.10	*2.56, 2.69*	$C^{\gamma}H$ 2.04; $C^{\varepsilon}H$ 2.14
Ala[17']	8.01	3.71	1.51	
Lys[18']	7.36	4.19	*1.92, 2.03*	$C^{\gamma}H$ 1.63
Lys[19']	8.51	4.67	*2.41, 1.92*	$C^{\gamma}H$ 1.38, 1.50; $C^{\delta}H$ 1.71; $C^{\varepsilon}H$ 3.02, 3.11; $N^{\zeta}H$ 7.61
Cys[20']	7.47	5.18	2.99	
Glu[21']	8.13	4.35	*2.14, 2.33*	$C^{\gamma}H$ 2.63, 2.73

TABLE I
(continued)

Residue	Chemical shift (ppm)			
	NH	$C^{\alpha}H$	$C^{\beta}H$	Other protons
$Gly^{22'}$	9.06	3.83, 407		
$Ser^{23'}$	8.80	4.21	3.89, 3.94	
$Ile^{24'}$	7.25	3.46	1.99	$C^{\gamma 1}H$ 1.41, 1.56; $C^{\gamma 2}H$ 0.57; $C^{\delta}H$ 0.84
$Ala^{25'}$	8.09	3.76	1.47	
$Thr^{26'}$	8.17	3.79	4.16	$C^{\gamma}H$ 1.19
$Met^{27'}$	7.25	3.96	*1.76*, *1.62*	$C^{\gamma}H$ 2.53, 2.70; $C^{\varepsilon}H$ 2.06
$Ile^{28'}$	7.94	3.23	1.66	$C^{\gamma 1}H$ 0.74; $C^{\gamma 2}H$ 0.73; $C^{\delta}H$ 1.05
$Lys^{29'}$	7.76	3.79	*1.93*, *1.86*	
$Lys^{30'}$	7.79	4.03	1.87	$C^{\gamma}H$ 1.57
$Lys^{31'a}$	7.84	4.06	*1.88*, *1.69*	$C^{\gamma}H$ 1.12; $C^{\delta}H$ 1.33
	7.87	4.02		
$Cys^{32'a}$	8.09	4.95	3.08, 3.15	
		4.99	3.06, 3.18	
$Asp^{33'}$	7.84	4.59	2.96, 2.96	
$Lys^{34'b}$	7.78	4.04	1.83	$C^{\gamma}H$ 1.45

SD was ±0.01 ppm. Underlined chemical shifts of $C^{\beta}H$ indicate a large (≥ 10 Hz) H-C^{α}-C^{β}-H vicinal coupling constant estimated from the DQF-COSY spectrum at 30 °C. For diastereotopic pairs of methylene protons or isopropyl methyl groups the stereospecific assignments are given (in italics) as far as they could be established. The first value is the shift of the proton or methyl group with the lower branch number.

[a] For $Lys^{31'}$ and $Cys^{32'}$ residues two sets of resonances were observed.

[b] Chemical shifts of $Lys^{34'}$ protons were measured at 30 °C.

ence of two slightly different conformations. The spin system of the C-terminal $Lys^{34'}$ was well resolved in the TOCSY spectrum at 30 °C, but not detectable in spectra at 10 °C. Due to the presence of a large number of lysine residues (14), some of their side-chain protons could not be assigned (Table 1).

Local structure analysis

The torsion angle constraints of Ea were determined by fitting the complete relaxation matrix of dipeptide unit protons (protons of a given residue and the NH proton of the next residue in the amino acid sequence) with experimental NOESY (τ_m = 100 ms) cross-peak integral

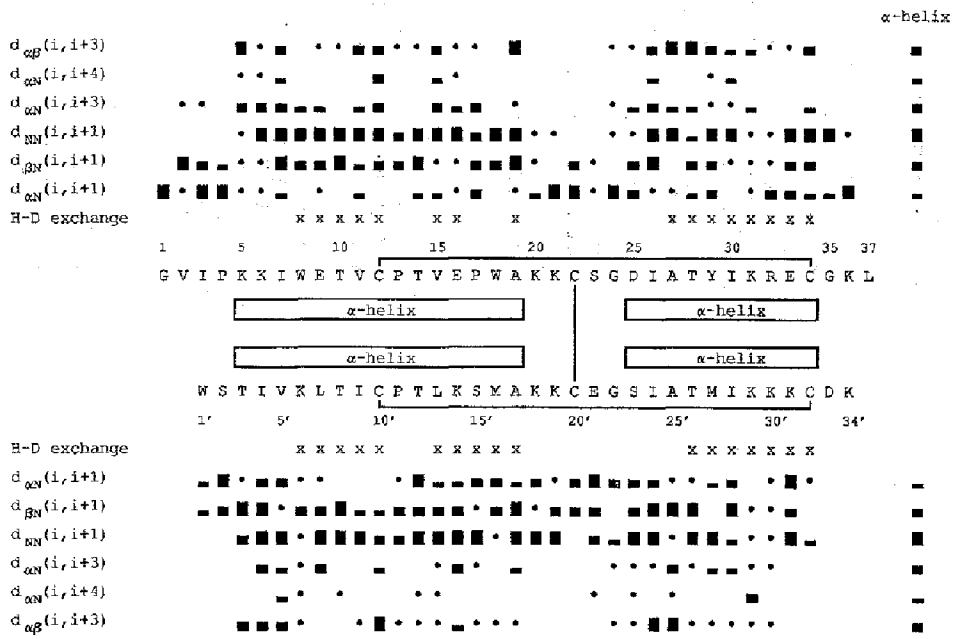

Fig. 3. Amino acid sequences of the A (top) and B (bottom) chains of Ea, the location of disulfide bonds and α-helical parts, survey of sequential NOE connectivities ($C^{\alpha}H$ protons of proline residues are considered as NH protons) and H-D exchange rate of amide protons. The one-letter code for amino acid residues is used. The residues with slowly exchanging amide protons (i.e., backbone NH protons exhibiting cross peaks in the NOESY spectrum recorded immediately after dissolving the sample in D_2O at 30 °C, pH 3.0) are indicated by crosses. The observed NOEs, classified as strong, medium and weak, are shown by thick, medium and thin bars, respectively. Filled circles indicate the cases where corresponding cross peaks could not be assigned unambiguously. To the right of the NOEs the pattern expected for residue i in a regular righthanded α-helix (Wüthrich, 1986) is shown for comparison. Four α-helical stretches, as deduced from NOE connectivities and deuterium exchange rates, are indicated by rectangles.

intensities, taking into account the sterically allowed values of φ and ψ torsion angles and information about $C^{\alpha}H$-$C^{\beta}H$ vicinal coupling constants. In this way, we obtained 126 torsion angle constraints (58 for φ, 42 for ψ, 17 for χ^1 and 9 for χ^2).

Preliminary structure calculations using distance geometry

Empirical distance calibrations were based on a $1/r^6$ dependence of cross-peak volume versus proton–proton distance. The strongest $d_{\alpha N}(i,i)$ and $d_{\alpha N}(i,i+1)$ NOESY cross peaks (τ_m = 100 ms) in α-helical stretches were used as reference values and assumed to have corresponding distances of 2.8 and 3.5 Å (the values for α-helices; see Wüthrich et al. (1984)). As no account was taken of spin diffusion at this stage, such a relationship tends to underestimate the upper limit for distance constraints. This mainly concerns side chains having geminal protons, therefore these protons were treated as pseudoatoms for preliminary calculations.

For the first DIANA run 692 upper limit constraints for proton–proton distances were used. To determine the configuration of X-Pro peptide bonds, a preliminary DIANA calculation was carried out with unconstrained torsion angles ω for proline residues.

Randomly generated starting conformations were optimized using the default 'standard strategy' of minimization (as it is called in the DIANA manual, version 1.14). After several REDAC iterations (each one from a random start, the output angle constraint file being used as input for the next run), various acceptable conformers were obtained.

The ω torsion angles for all proline residues were in the range 180 ± 30° in all obtained conformations. In subsequent DIANA calculations, the ω torsion angles of proline residues were fixed at 180°.

Location of disulfide and hydrogen bonds

No free SH groups were found in Ea (Arseniev et al., 1994). Thus, three disulfide bonds were expected. Analysis of the S-S distance distribution after preliminary DIANA calculations (Table 2) yields only one possibility for the three disulfide bridges: Cys^{22}-$Cys^{20'}$, Cys^{12}-Cys^{34} and $Cys^{10'}$-$Cys^{32'}$. Upper (3.1 Å for C^{β}-S^{γ} and 2.1 Å for S^{γ}-S^{γ} distances) and lower (3.0 Å for C^{β}-S^{γ} and 2.0 Å for S^{γ}-S^{γ} distances) distance constraints for these disulfide bridges were used in subsequent calculations.

TABLE 2
DISTRIBUTION OF DISTANCES (Å) BETWEEN S^{γ} ATOMS OF CYSTEINE RESIDUES OVER 10 STRUCTURES OBTAINED AFTER PRELIMINARY DIANA CALCULATION

Residue number	12	22	34	10'	20'	32'
12		9.07	1.84	14.0	8.58	11.4
22	15.7		14.6	14.8	1.88	10.3
34	6.04	19.2		14.4	16.2	13.7
10'	15.3	17.3	16.7		15.6	4.23
20'	16.3	2.14	19.8	18.0		11.7
32'	13.8	14.6	17.8	10.8	14.6	

The values of minimal and mean distances are shown above and below the diagonal, respectively. The underlined values correspond to residues forming disulfide bonds.

From a qualitative analysis of d-connectivities (Fig. 3) and inspection of conformations ob-tained after preliminary DIANA calculations, it was clear that each chain of Ea forms two helical regions (Lys^5-Ala^{19} and Asp^{25}-Cys^{34}; $Thr^{3'}$-$Ala^{17'}$ and $Ser^{23'}$-$Cys^{32'}$, see Fig. 3). We assumed that the 29 slowly exchanging amide protons form hydrogen bonds of α-helical type (NH_i-OC_{i-4}). Slowly exchanging amide protons near the N-terminus of each α-helix can form a 3_{10}-helix-type hydrogen bond (NH_i-OC_{i-3}). No constraints were included for such hydrogen bonds. In subsequent calculations, 58 upper (3.0 Å for O-N and 2.0 Å for O-HN) and 58 lower (2.7 Å for O-N and 1.8 Å for O-HN) distance constraints were used for 29 hydrogen bonds.

Additional assignment of ambiguously assigned and overlapped cross peaks

To check the reliability of the input data, we used the set of preliminary DIANA conformations for semiautomatic assignment of cross peaks. On the basis of the resonance assignments (Table 1), all possible variants of cross-peak assignment were listed and then, if the minimal distance between the two protons over the group of previously obtained conformations was less than a cutoff distance of 6 Å, such an assignment was considered to be possible. If several possible assignments were left for a cross peak, then this peak was assigned using lineshape, precise values of chemical shifts, and the interproton distance distribution in previously obtained structures. After assignment updating, we repeated the peak integration, MARDIGRAS calibration of distance constraints and the DIANA calculation. To obtain a self-consistent data set, the procedure was repeated 10 times. In Fig. 4 these NOE data are summarized in the form of a diagonal plot.

Distance constraints calculation using MARDIGRAS

It has been demonstrated that the use of a complete relaxation matrix analysis of NOESY intensities yields more accurate distance constraints than the isolated spin-pair approximation (Keepers and James, 1984; Borgias and James, 1988,1990; Thomas et al., 1991). In this study, MARDIGRAS (Matrix Analysis of Relaxation for DIscerning Geometry in solution) was used to determine accurate upper and lower constraints for proton–proton distances from the NOESY cross-peak intensities. Preliminary calculations were carried out independently based on two sets of data (mixing times 100 and 200 ms). Shorter mixing times give more accurate constraints for methylene

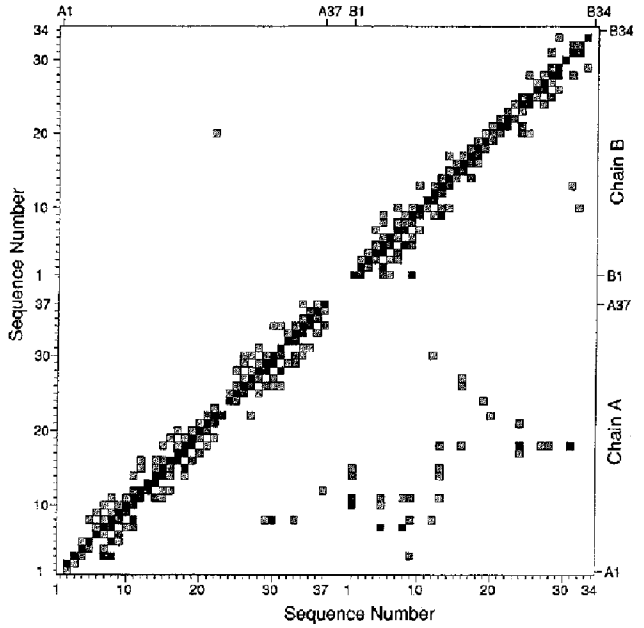

Fig. 4. Diagonal plot representing the survey of NOE contacts observed for Ea. A filled square in position (i,j) of the plot indicates that between the two residues in the sequence locations i and j one or several NOE contacts were observed. The darkness of the squares indicates the number of contacts – from one (light grey) to 10 or more (black). The lower right part of the plot includes contacts between all atoms; the upper left contains only backbone–backbone NOE contacts.

groups and facilitate stereospecific assignment. However, the number of peaks in the 200 ms spectrum was greater than in the 100 ms spectrum, so for final calculations we used data from the 200 ms spectrum.

The MARDIGRAS algorithm requires knowledge of correlation times and an estimate of the spectral noise level. We used a correlation time of 6 ns, estimated from the molecular weight of ectatomin and the solvent viscosity. The noise level in the NOESY spectra was estimated by integration of several spectral regions containing no protein signals. We took the maximum of the absolute value of this integral as the noise level. After MARDIGRAS normalization, noise levels were 0.02 and 0.04 for the 200 and 100 ms NOESY spectra, respectively. The number of constraints obtained using MARDIGRAS was less than the number of unambiguously assigned cross peaks, because some cross peaks belong to protons with a fixed distance between them and for some weak cross peaks, MARDIGRAS could not determine distance constraints due to significant spin diffusion. At the final stage (after 10 rounds of DIANA calculations and assignment procedures) we obtained 755 upper and lower distance constraints (404 intraresidue, 178 sequential, 92 medium-range, 29 long-range and 52 interchain).

Additional lower-bound distance constraints were obtained from qualitative analysis of sequential d_{NN} connectivities (Fig. 3). The absence of a cross peak between NH protons of adjacent residues was interpreted as indicating that the distance between these protons is greater than 3.5 Å. The cutoff value of 3.5 Å was selected on the basis of distances obtained for weak cross peaks by MARDIGRAS. Thus, the hinge regions of Ea were additionally constrained.

The distance constraints obtained using MARDIGRAS were used, together with hydrogen and disulfide bond constraints, in the final DIANA calculation.

Structure calculation using distance geometry

The procedure used in the second round of DIANA structure calculations was similar to that of the preliminary calculation. After several REDAC cycles, each one starting from 50 random conformations, new, more narrow, angle constraints were determined. These additional constraints improved convergence and were not systematically violated during subsequent steps.

Stereospecific assignments for protons in methylene and isopropyl methyl groups were determined using GLOMSA. These assignments were made for two α-methylene, 28 β-methylene, seven γ-methylene, three δ-methylene and three isopropyl groups (Table 1).

The final set of Ea conformations was obtained using DIANA with the stereospecific assignments from GLOMSA and the additional angle constraints obtained using the REDAC algo-rithm. A total number of 822 upper (755 NOE, 58 H-bonds and 9 S-S bonds) and 825 lower distance constraints was used (three additional

TABLE 3
ANALYSIS OF THE 20 BEST DIANA STRUCTURES

Parameter	Quantity	Unit	Values
Final target function[a]		Å²	4.89 ± 0.34
Number of constraints	NOE		755
	H-bond		58
	S-S bond		9
	dihedral angles		215
Upper constraint violations	Number > 0.2 Å		11 ± 3
	Maximum	Å	0.41 ± 0.03
	Sum	Å	8.34 ± 0.54
Lower constraint violations	Number > 0.2 Å		13 ± 2
	Maximum	Å	0.57 ± 0.04
	Sum	Å	7.99 ± 0.53
van der Waals constraint violations	Number > 0.2 Å		2 ± 1
	Maximum	Å	0.27 ± 0.04
	Sum	Å	7.14 ± 0.65
Angle constraint violations	Number > 5°		2 ± 1
	Maximum	degree	5.94 ± 0.97
	Sum	degree	68.21 ± 8.91

The average values and SDs are given.

[a] Target function values were calculated with the following weight factors: 1 for upper and lower distance constraints, 2 for van der Waals constraints and 5 Å² for angle constraints.

TABLE 4
MEAN, MINIMUM AND MAXIMUM CHARMm POTENTIAL ENERGY VALUES FOR 20 FINAL REFINED STRUCTURES OF Ea

	E_{TOT}	E_{VDW}	E_{BOND}	E_{ANGLE}	E_{IMPR}	E_{DIHED}	E_{ELEC}
Mean	−868	−1454	31.9	230	3.8	344	−24
SD	31	27	0.4	6	0.4	20	3
Min	−939	−1502	30.7	217	3.3	306	−29
Max	−803	−1391	32.6	241	4.8	392	−19

The potential energies are: E_{TOT}, total potential energy; E_{VDW}, energy due to van der Waals interactions calculated from a Lennard-Jones equation; E_{BOND}, E_{ANGLE}, E_{IMPR} and E_{DIHED}, potential energies due to covalent geometry and 1–4 interactions; E_{ELEC}, electrostatic potential energy calculated using a dielectric constant of 80 and a distance-dependent dielectric approximation. The standard deviation of the mean is given. All energies are given in kJ/mol.

constraints were obtained from qualitative analysis of sequential d_{NN} connectivities, see above). The total number of angle constraints was 215 (64 for φ, 68 for ψ, 54 for χ^1, 23 for χ^2, four for χ^3 and two for χ^4). Out of 200 DIANA structures calculated from random starting seed, we chose the 20 with the lowest penalty functions. The values of penalty functions as well as distance and angle constraint violations for these 20 structures and their rmsd values are summarized in Table 3.

Energy refinement of the Ea structure

The 20 best structures were refined using unrestrained energy minimization with CHARMm. The R and R^x factors (see Materials and Methods) varied only slightly during minimization (Table 5). The rmsd between backbone torsion angles before and after energy minimization is 19°, while the maximum angle difference is 84°. Angle differences greater than 40° were observed in the non-helical parts of both chains and near proline residues. Such differences indicate that some conformations obtained by DIANA are far from energy minima and so energy minimization was necessary.

The local rmsd of the hinge regions (Fig. 5) increased after energy minimization. This occurs because conformations obtained by DIANA lie between several energy minima and conformations reach one or another minimum during minimization.

A scatter plot of φ, ψ and χ^1 angles, which demonstrates the quality of the structures, is presented in Fig. 6. The potential energies of the final (energy-minimized) structures are of reasonable magnitude and exhibit small deviations between structures (Table 4). The low values of the electrostatic potential energies are due to the large dielectric constant and distance-dependent dielectric approximation used for the final energy minimization. The distributions and conformations of the charged or polar side chains are of particular interest in this protein, hence we used a very weak electrostatic term to ensure that any conformational preference amongst the structures reflects only the experimental NOE data and steric interactions. Additional parameters characterizing the set of structures obtained are listed in Table 5. The mean values of the R and R^x factors (Table 5) clearly show that the structures agree well with the NOE data. Superpositions of the structures obtained are shown in Figs. 7 and 8.

Circular dichroism spectroscopy

Far UV circular dichroism offers a good quantitative measure of the secondary structure content of proteins. Since we know the spatial structure of Ea in aqueous solution and the ability of the Ea molecule to incorporate in the membrane bilayer, it is interesting to compare the CD spectra of Ea in water and in methanol (a solvent that mimicks the environment of a membrane).

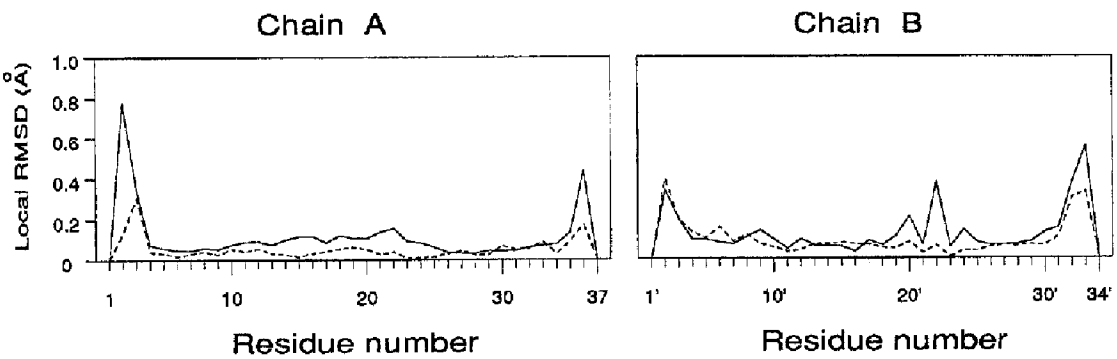

Fig. 5. Plots of local rmsd versus the amino acid sequence of 20 structures before (dashed line) and after (solid line) CHARMm energy minimization. Local rmsd values of backbone heavy atoms for segments of three residues were obtained after a local best fit of the corresponding segment. Rmsd values are plotted at the position of the central residue.

Figure 9 shows the CD spectra of Ea in water and in methanol. The Ea spectrum in water has two minima (at 207 and 222 nm) and a maximum at 193 nm, highly indicative of helical conformation (Greenfield and Fasman, 1969). The content of α-helix, deduced from quantitative analysis of this CD spectrum to be 65%, is in good agreement with the structure obtained using NMR data.

The change in solvent polarity caused a negligible change in the CD spectrum near 225 nm. This change may be caused by increased light scattering due to oligomerization of Ea or by minor changes in secondary structure of the molecule. The similarity of the CD spectra in methanol and water suggests that Ea retains predominantly an α-helical conformation in both solvents.

Discussion

The Ramachandran plot of all 20 structures (Fig. 10) shows that the majority of φ,ψ angle combinations are in favourable regions; only Gly^{24} and $Gly^{22'}$ residues lie outside these regions. Analysis of φ,ψ distributions (Fig. 6) and local rmsd (Fig. 5) shows that the backbone structure of the helical regions (Lys^{5}-Lys^{20}, Asp^{25}-Gly^{35} (chain A) and $Thr^{3'}$-$Lys^{18'}$, $Ser^{23'}$-$Cys^{32'}$ (chain B)) was well defined. The conformations of the hinge regions (Lys^{21}-Gly^{24} (chain A) and $Lys^{19'}$-$Gly^{22'}$ (chain B)) are less well defined. Several backbone structures of hinge regions obtained after CHARMm refinement may reflect the dynamic behavior of the protein in solution, but can be explained by drawbacks in the structure calculation

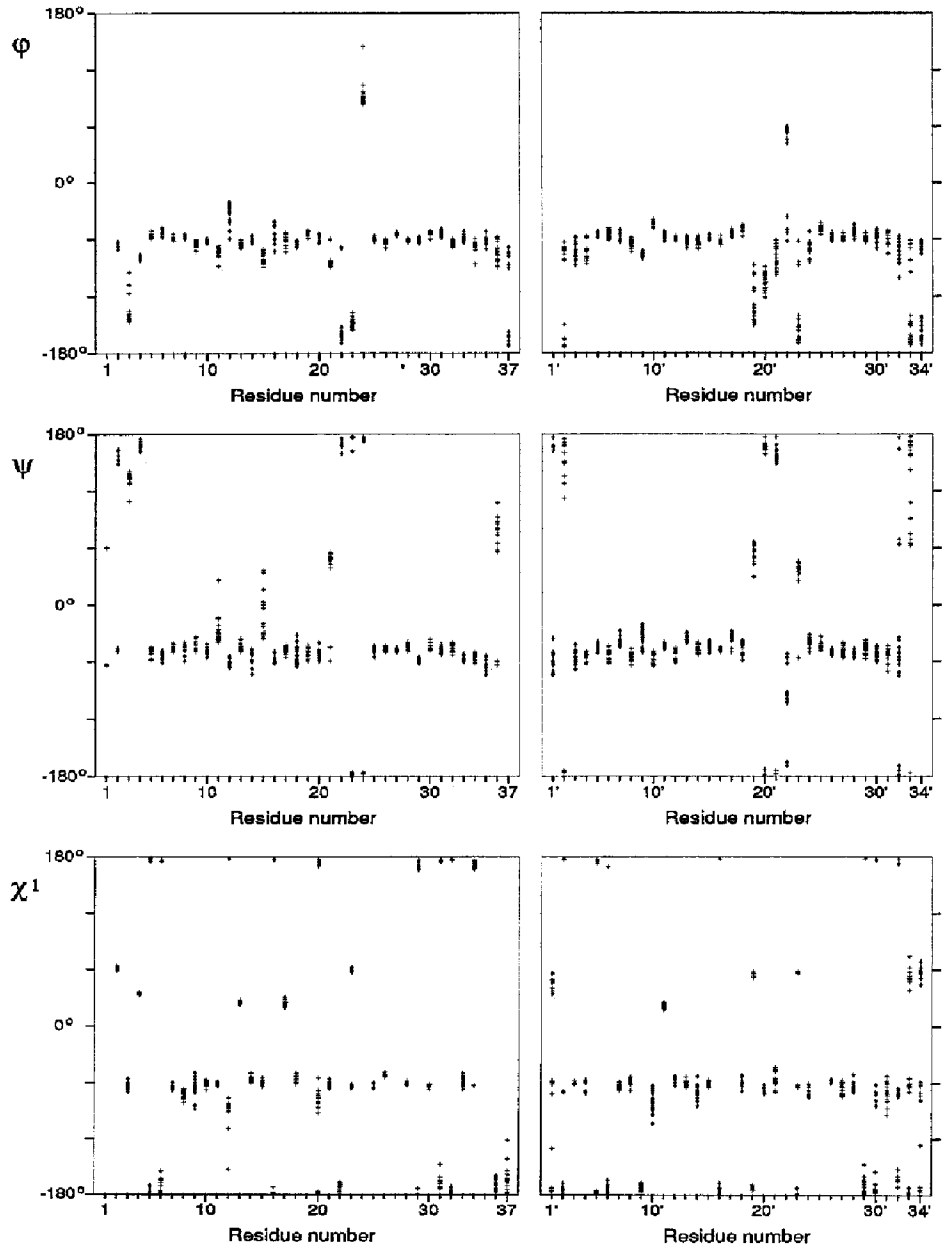

Fig. 6. Plots of φ, ψ and χ^1 angles of 20 CHARMm-refined structures versus the amino acid sequence of Ea.

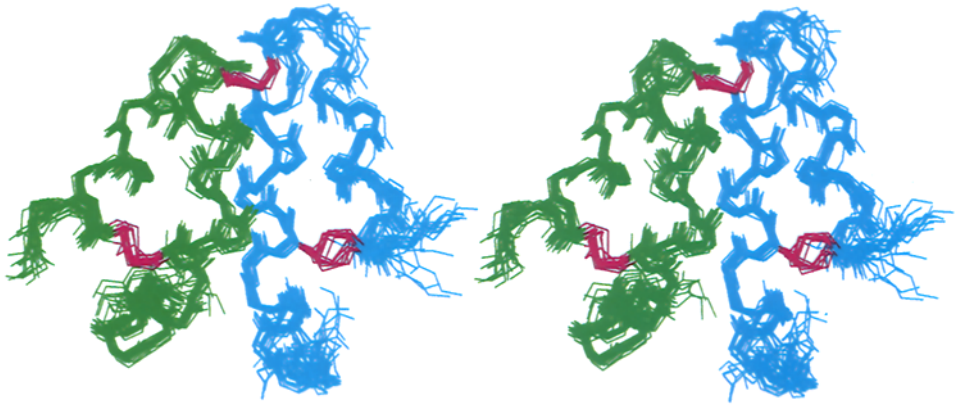

Fig. 7. Stereoview of 20 CHARMm-refined structures. The superposition has minimum rmsd of backbone heavy atoms of residues 5–34 (chain A, green) and 3'–32' (chain B, cyan). All backbone heavy atoms and heavy atoms of cysteine residues are shown. Disulfide bonds are magenta.

methods used. The N- and C-termini of both chains also display several conformations and are probably mobile.

Both chains have a similar structure (Fig. 7) which is consistent with their high sequence homology (Fig. 3). Each chain consists of two antiparallel α-helices (Lys^{5}-Lys^{20}, Asp^{25}-Gly^{35} (chain A) and $Thr^{3'}$-$Lys^{18'}$, $Ser^{23'}$-$Cys^{32'}$ (chain B)). The hinge regions connecting the α-helices (Lys^{21}-Gly^{24} and $Lys^{19'}$-$Gly^{22'}$) are less well defined than the helical regions. Residues Cys^{22}, Ser^{23}, $Cys^{20'}$ and $Glu^{21'}$ are in 'extended' conformations; this means that the chains turn gradually, rather than sharply. All the NH protons of Ea which have a slow deuterium exchange rate belong to the α-helical parts of the molecule and take part in intramolecular hydrogen bonds.

All four helices are amphipathic. The helix Lys^{5}-Lys^{20} contains two proline residues (Pro^{13} and Pro^{17}) which distort the α-helical structure. Both proline residues introduce kinks in the helix axis of about 40°. The helix $Thr^{3'}$-$Lys^{18'}$ is also distorted by a proline residue ($Pro^{11'}$ causes a kink of about 30°). The amide protons of the residues adjacent to prolines do not form hydrogen bonds and exhibit fast deuterium exchange (Fig. 3). A substantial part of the molecular surface is positively charged, due to the large number of surface lysine side chains. This suggests that Ea may interact with negatively charged molecules. Most lysine side chains are exposed to the solvent and mobile. This explains the equality of chemical shifts of geminal side-chain protons for most lysine residues (Table 1). The mobility of nonpolar side chains of the molecule in aqueous solution is restricted, due to hydrophobic interactions between the α-helices. Nonpolar amino acid residues form a hydrophobic core of the protein. The side chains of Glu^{16} and Lys^{20} form a salt bridge which stabilizes the last turn of the helix.

The three disulfide bridges play an important role in the Ea structure. Two intrachain disulfide bridges (Cys^{12}-Cys^{34} and $Cys^{10'}$-$Cys^{32'}$) connect the ends of the antiparallel α-helices and stabilize their relative positioning. The third disulfide bridge (Cys^{22}-$Cys^{20'}$) connects the two hinge regions. Thus, this four-helical bundle is essentially stabilized by electrostatic, hydrophobic and other nonbonded interactions between the α-helices. The interchain

TABLE 5
ANALYSIS OF THE 20 DIANA STRUCTURES BEFORE AND AFTER ENERGY REFINEMENT

	Pairwise Rmsd (Å)			
	Before refinement		After refinement	
Residues	Backbone heavy atoms	All heavy atoms	Backbone heavy atoms	All heavy atoms
1–37 and 1'–34'	1.18 ± 0.26	1.72 ± 0.27	1.25 ± 0.27	1.84 ± 0.28
5–34 and 3'–32'	0.60 ± 0.16	1.25 ± 0.18	0.75 ± 0.21	1.38 ± 0.19
1–37	0.84 ± 0.31	1.26 ± 0.20	0.83 ± 0.27	1.34 ± 0.20
5–34	0.34 ± 0.11	1.07 ± 0.16	0.46 ± 0.14	1.17 ± 0.17
1–34'	1.19 ± 0.34	1.92 ± 0.41	1.35 ± 0.35	2.10 ± 0.41
3'–32'	0.58 ± 0.18	1.24 ± 0.24	0.77 ± 0.22	1.41 ± 0.23
5–20	0.24 ± 0.08	1.04 ± 0.22	0.40 ± 0.13	1.16 ± 0.22
25–34	0.22 ± 0.10	1.00 ± 0.27	0.20 ± 0.07	0.98 ± 0.31
3'–18'	0.46 ± 0.16	0.90 ± 0.22	0.49 ± 0.16	1.00 ± 0.22
23'–32'	0.32 ± 0.18	1.17 ± 0.19	0.52 ± 0.15	1.34 ± 0.21

The average pairwise rmsd values and SDs are given for the 20 structures. Before refinement, the R factor was 0.510 ± 0.007 and the R^{λ} factor was 0.128 ± 0.003; after refinement, these values were 0.508 ± 0.009 and 0.138 ± 0.006, respectively.

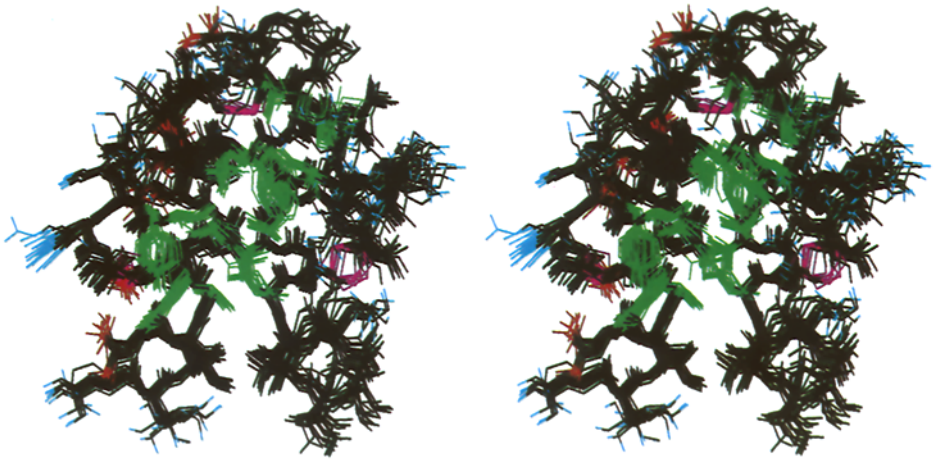

Fig. 8. Stereoview of a superposition of 20 CHARMm-refined structures with minimum rmsd of the backbone heavy atoms of residues 5–34 and 3'–32'. All heavy atoms of these residues are shown. Positively charged groups are coloured cyan, negatively charged groups red, side chains forming a hydrophobic core green, disulfide bonds magenta and other atoms black.

disulfide bridge (Cys^{22}-$Cys^{20'}$) has a left-handed conformation in all 20 structures obtained ($\chi^3 = -80.6 \pm 3.4°$). The conformation of this disulfide bridge is well defined, due to the presence of NOE cross peaks between the $C^{\alpha}H$ protons of the cysteine residues. The conformations of the intrachain disulfide bridges are less well defined, due to the absence of NOE cross peaks between these cysteine residues. In three out of 20 structures the conformation of the Cys^{12}-Cys^{34} disulfide bridge changed during energy minimization. This may be due to a limitation in the minimization protocol, or the presence of several conformations of this disulfide bridge. The third disulfide bridge ($Cys^{10'}$-$Cys^{32'}$) has two conformations (left- and right-handed), nearly uniformly distributed amongst the 20 energy-refined structures obtained. This is consistent with the two distinct sets of resonances observed for $Cys^{32'}$ and $Lys^{31'}$ (Table 1).

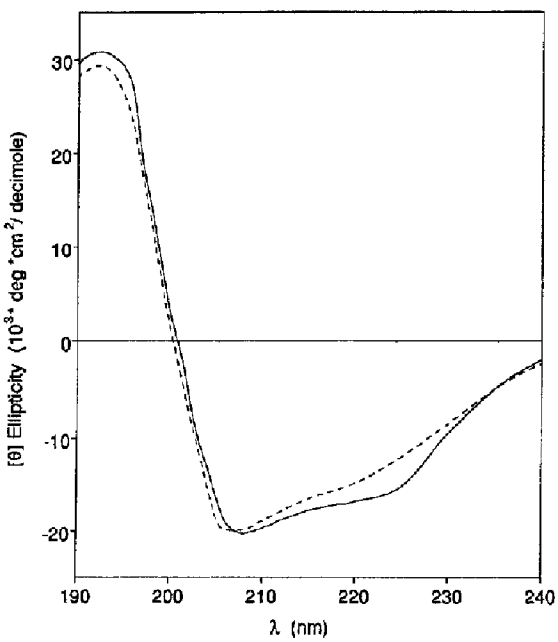

Fig. 9. CD spectra of Ea in water (solid line) and in methanol (dashed line).

The structure of Ea has a four-helical bundle motif. Currently known proteins which incorporate this motif as their dominant structure feature include (i) the haemerythryn subunit and related monomeric myohaemerethryn derived from marine worms (Hendrickson et al., 1975); (ii) the apoferritin monomer (Banyard et al., 1978); (iii) tobacco mosaic virus coat protein (Bloomer et al., 1978); (iv) *E. coli* cytochrome b_{562} (Mathews et al., 1979); and (v) the dimeric cytochrome *c'* from *Rhodospirillum molischianum* (Weber et al., 1980) and some other proteins (Chou et al., 1988). These proteins have widely different functions. However, the following basic features are common to most four-helical bundles (Chou et al., 1988) including our Ea structure: the four helices form an assembly with an approximately rhombic cross section; the orientation of neighboring helices is nearly, but not exactly, antiparallel; and the helices are tilted in such a way that the bundle has a left-handed twist (Weber and Salemme, 1980; Chou et al., 1988).

In a preceding paper (Arseniev et al., 1994) we reported that Ea can form a membrane pore or ion channel. It is obvious that a significant conformational reorganization of Ea is necessary before it can incorporate in a lipid bilayer. In Fig. 11, we present two possible models for Ea folding into a membrane bilayer, based on the following assumptions: (i) the channel is dimeric (this is evident from the second-order concentration dependence of channel activity in vitro in planar bilayer membranes; see Arseniev et al. (1994)); (ii) the secondary structure of Ea and the relative positions of pairs of helices belonging to the same chain should be similar in aqueous solution and in the membrane bilayer (see the results of the CD measurement and the Discussion above); (iii) the length

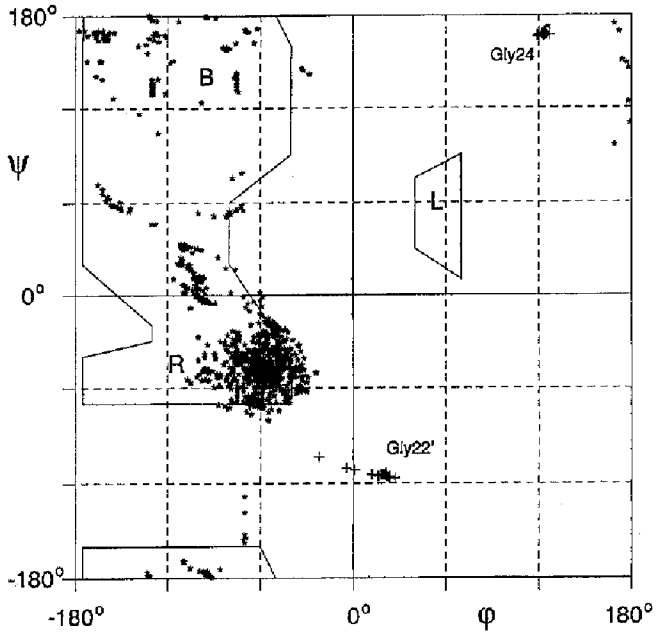

Fig. 10. Ramachandran φ,ψ plot for all residues in the 20 energy-refined structures of Ea. Glycine residues are indicated by '+'.

of Ea helices (from 15 to 25 Å) is insufficient to span the membrane bilayer (≥30 Å). At the first stage, lipid molecules destroy the hydrophobic and electrostatic interactions between the A and B chains of Ea and the chains separate. It is likely that after this stage a deployed Ea molecule sticks to the membrane surface, such that the hydrophobic surfaces of the amphiphilic helices are submerged into the lipid bilayer (Fig. 11A). Then the two Ea molecules dimerize and penetrate into the lipid bilayer. There are many ways in which two Ea molecules can form a dimer in a membrane bilayer. Two possibilities are presented in Figs. 11B and C. To understand the arrangement of the channel structure, we need additional experimental data about Ea regions: which are exposed from the lipid bilayer, and which regions form the dimer. This work is currently in progress.

The membrane insertion mechanism described above resembles the inside-out mechanism proposed for the action of colicin, a pore-forming toxin produced by *E. coli* (Parker et al., 1992). In both cases insertion occurs without change in secondary structure of the proteins, and channels are formed by assembly of α-helices. The conformations of these proteins in the absence of a transmembrane voltage (a deployed molecule, see Fig. 11A, and an 'umbrella' model, see Parker et al. (1992)) are also somewhat similar: amphipathic helices stay embedded on the membrane surface. A noticeable difference between colicin and ectatomin structures is that the colicin molecule contains a hydrophobic helical hairpin, which promotes spontaneous insertion of proteins into the lipid bilayer (Engelman and Steitz, 1981), whereas the ectatomin molecule does not incorporate hydrophobic helices.

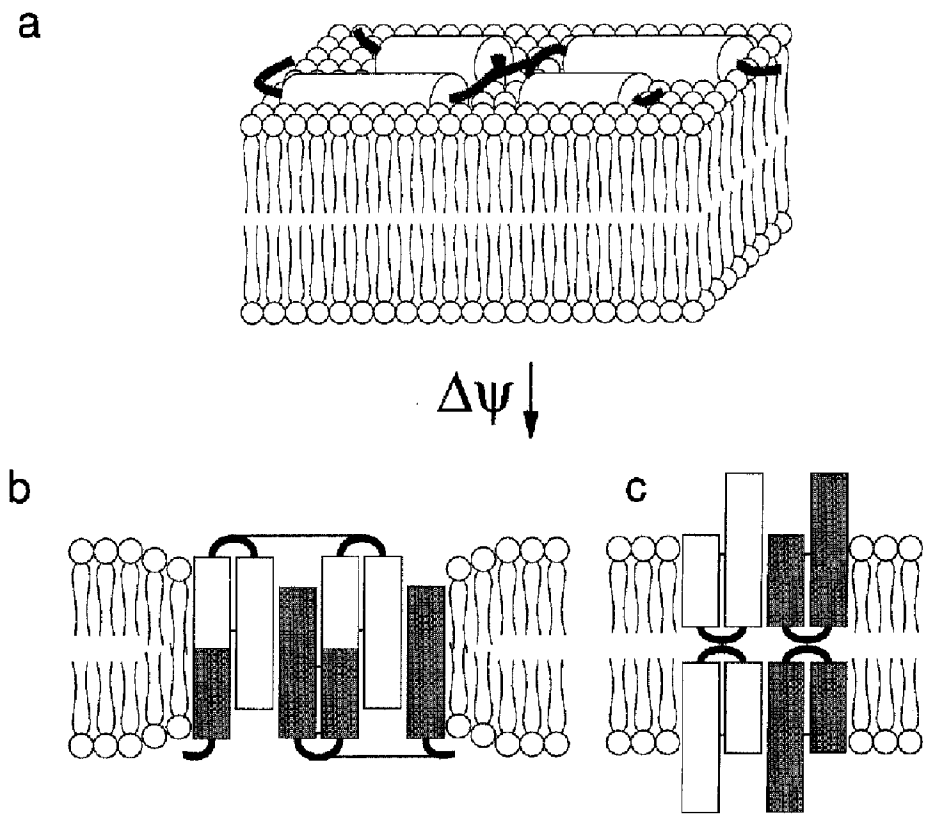

Fig. 11. Model for protein insertion into membranes, suggested by the structure of Ea in water solution. (A) Surface-bound Ea molecule; (B) and (C) two possible ways of ectatomin dimerization and pore forming in the presence of membrane potential Δψ.

Thus, the energy cost of disrupting the three-dimensional fold of ectatomin would be balanced by the replacement of hydrophobic interactions within the protein by interactions between the helical surfaces and the lipid bilayer.

Conclusions

We have determined the structure of Ea in aqueous solution, employing a distance geometry approach based on accurately determined upper and lower distance constraints obtained using MARDIGRAS and unrestrained energy minimization with the CHARMm force field. The presence of four amphipathic α-helices suggests that Ea may be able to incorporate in a membrane bilayer without an appreciable change in its secondary structure.

Acknowledgements

We thank Dr. I.A. Kudelina for assistance in recording and analysis of CD spectra. We are also grateful to the referees for their critical revision of the manuscript.

References

Arseniev, A.S., Pluzhnikov, K.A., Nolde, D.E., Sobol, A.G., Torgov, M.Yu., Sukhanov, S.V. and Grishin, E.V. (1994) *FEBS Lett.*, **347**, 112–116.

Banyard, S.H., Stammers, D.K. and Harrison, P.M. (1978) *Nature*, **271**, 282–284.

Barsukov, I.L., Nolde, D.E., Lomize, A.L. and Arseniev, A.S. (1992) *Eur. J. Biochem.*, **206**, 665–672.

Bloomer, A.C., Champness, J.N., Bricogne, G., Staden, R. and Klug, A. (1978) *Nature*, **276**, 362–368.

Blum, M.S. (1992) *J. Toxicol.*, **11**, 115–164.

Borgias, B.A. and James, T.L. (1988) *J. Magn. Reson.*, **79**, 493–512.

Borgias, B.A. and James, T.L. (1990) *J. Magn. Reson.*, **87**, 475–487.

Brooks, B.R., Brucoleri, R.E., Olafson, B.D., States, D.G., Swaminathan, S. and Karplus, M. (1988) *J. Comput. Chem.*, **4**, 187–217.

Chou, K.-C., Maggiora, G.M., Nemethy, G. and Scheraga, A. (1988) *Proc. Natl. Acad. Sci. USA*, **85**, 4295–4299.

Eccles, S., Güntert, P., Billeter, M. and Wüthrich, K. (1991) *J. Biomol. NMR*, **1**, 111–130.

Engelman, D.M. and Steitz, T.A. (1981) *Cell*, **23**, 411–422.

Greenfield, N. and Fasman, G.D. (1969) *Biochemistry*, **8**, 4108–4116.

Güntert, P., Qian, Y.Q., Otting, G., Müller, M., Gehring, W. and Wüthrich, K. (1991) *J. Mol. Biol.*, **217**, 531–540.

Güntert, P. and Wüthrich, K. (1991) *J. Biomol. NMR*, **1**, 447–456.

Hendrickson, W.A., Klippenstein, G.L. and Ward, K.B. (1975) *Proc. Natl. Acad. Sci. USA*, **72**, 2160–2164.

Keepers, J.W. and James, T.L. (1984) *J. Magn. Reson.*, **57**, 404–426.

Lomize, A.L., Sobol, A.G. and Arseniev, A.S. (1990a) *Bioorg. Khim. (Russia)*, **16**, 179–201.

Lomize, A.L., Arseniev, A.S., Maslennikov, I.V. and Bystrov, V.F. (1990b) *Bioorg. Khim. (Russia)*, **16**, 1310–1324.

Lomize, A.L., Pervushin, K.V. and Arseniev, A.S. (1992) *J. Biomol. NMR*, **2**, 361–372.

Mathews, F.S., Bethge, P.H. and Czerwinski, E.W. (1979) *J. Biol. Chem.*, **254**, 1699–1706.

Parker, M.W., Postma, J.P.M., Pattus, F., Tucker, A.D. and Tsernoglou, D. (1992) *J. Mol. Biol.*, **224**, 639–657.

Pluzhnikov, K.A., Nolde, D.E., Tertishnikova, S.M., Sukhanov, S.V., Sobol, A.G., Torgov, M.Yu., Filippov, A.K., Arseniev, A.S. and Grishin, E.V. (1994) *Bioorg. Khim. (Russia)*, **20**, 857–871.

Schmidt, J.O., Blum, M.S. and Overal, W.L. (1986) *Toxicon*, **24**, 907–921.

Thomas, P.D., Basus, V.J. and James, T.L. (1991) *Proc. Natl. Acad. Sci. USA*, **88**, 1237–1241.

Weber, P.C., Bartsch, R.G., Cusanovich, M.A., Hamlin, R.C., Howard, A., Jordan, S.R., Kamen, M.D., Meyer, T.E., Weatherford, D.W., Xuong, N.H. and Salemme, F.R. (1980) *Nature*, **286**, 302–304.

Weber, P.C. and Salemme, F.R. (1980) *Nature*, **287**, 82–84.

Wüthrich, K., Billeter, M. and Braun, W. (1984) *J. Mol. Biol.*, **180**, 715–740.

Wüthrich, K. (1986) *NMR of Proteins and Nucleic Acids*, Wiley, New York, NY.